PROCEEDINGS OF SCIENCE

Simulation of the instrument performance of the Antarctic Demonstrator for the Advanced Particle-astrophysics Telescope in the presence of the MeV background

Wenlei Chen[a,*] **and James H. Buckley**[b] **for the APT collaboration**

[a] *University of Minnesota, Twin Cities*
School of Physics and Astronomy, 116 Church Street SE, Minneapolis, MN 55455, USA
[b] *Washington University in St. Louis,*
Dept. Physics, One Brookings Drive, Saint Louis, MO, USA

E-mail: chen6339@umn.edu, ...

The Advanced Particle-astrophysics Telescope (APT) is a mission concept of a next-generation space-based gamma-ray and cosmic-ray observatory. We present the simulation of the instrument performance of the Antarctic Demonstrator for APT (ADAPT), a proposed long-duration balloon instrument based on a small portion of the full APT detector. We construct a semianalytical model of the MeV-GeV background for ADAPT based on observations from previous high-altitude balloon experiments and simulations of the upper atmosphere. We find that the ADAPT background is dominated by the gamma-ray albedo of the earth's atmosphere. In the presence of this background, we simulate a detector design based on a 45 cm × 45 cm detector composed of 8 thin layers of CsI:Na scintillators. We develop and optimize reconstruction algorithms for gamma-rays from a few hundreds of keV up to a few GeV energies. We present results of a complete off-line analysis to derive the best reconstruction methods. At photon energies from 30 MeV to a few GeV, ADAPT could provide degree-level to sub-degree-level observations of galactic and extragalactic gamma-rays with an effective area of above 0.05 m^2. In the MeV regime, our simulation shows that ADAPT can achieve a degree-level localization accuracy for gamma-ray bursts down to about 1 MeV/cm^2 in the presence of the gamma-ray and cosmic-ray background. ADAPT would be able to detect a few GRBs during the planned Antarctic balloon flight.

38th International Cosmic Ray Conference (ICRC2023)
26 July - 3 August, 2023
Nagoya, Japan

*Speaker

PoS(ICRC2023)841

1. Antarctic Demonstrator for the Advanced Particle-astrophysics Telescope

The Advanced Particle-astrophysics Telescope (APT) is a mission concept of a gamma-ray and cosmic-ray observatory in an orbit around the second sun-Earth Lagrange point (L2). With a multiple-layer tracker and an imaging calorimeter, APT is designed to observe gamma-rays at energies from hundreds of keV up to a few TeV. Aiming at maximizing effective area and field of view for MeV-TeV gamma-ray and cosmic-ray measurements, the current APT detector design is based on 3-meter scintillating fibers read out by Silicon photomultipliers (SiPMs). The APT detector includes a multiple-layer tracker composed of scintillating fibers and an imaging calorimeter composed of thin layers of sodium-doped CsI (CsI:Na) scintillators and wavelength-shifting (WLS) fibers. Crossed planes of WLS fibers are attached on top and bottom of the CsI:Na crystals to measure and localize energy deposition.

The Antarctic Demonstrator for APT (ADAPT) is a high-altitude balloon experiment scheduled to fly during the 2025–2026 summer window in the Antarctic. The ADAPT detector uses only $\sim$ 1% of the total amount of sensitive materials used in the full APT detector. The ADAPT experiment is aimed to demonstrate the potential of the APT instrument and test our gamma-ray and cosmic-ray reconstruction algorithms. The mission will provide real-time alerts and localization of gamma-ray bursts (GRBs) and other gamma-ray transients that occur during the long-duration Antarctic flight. As shown in Fig. 1, the sensitive detector of ADAPT consists of 4 fully instrumented tracker/imaging-CsI-calorimeter (ICC) layers and 4 additional CsI-calorimeter layers on bottom to increase the radiation length of the instrument. Each CsI-calorimeter layer includes 3×3 tiles of 15cm $\times$ 15cm $\times$ 5mm CsI:Na crystals. The design will achieve a $\sim 1/2$ meter square aperture for gamma-ray and cosmic-ray observations. We simulate gamma-ray and cosmic-ray events for the ADAPT detector using `Geant4` [1]. Detailed descriptions of the APT and ADAPT science goals and instrument design can be found in [2–4]. The project status of APT and ADAPT missions is described in [4].

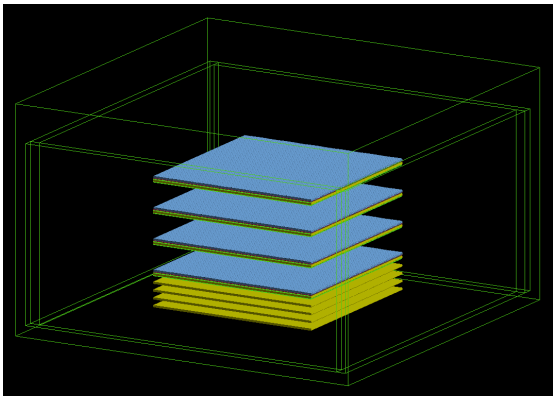

Figure 1: Geometry of the ADAPT payload and sensitive detector for the `Geant4` [1] simulation. The ADAPT sensitive detector consists of 4 fully instrumented ICC layers and 4 additional CsI-calorimeter layers on bottom.

As a high-altitude balloon mission, ADAPT will experience a strong background of gamma-ray and cosmic-ray radiation produced near the Earth. The background is dominated by atmospheric gamma-ray radiation and terrestrial cosmic-ray emission. In this paper, we describe a semi-analytical model of the gamma-ray and cosmic-ray background for ADAPT based on observations from previous high-altitude balloon experiments and simulations of the upper atmosphere. We present the ADAPT performance of the GRB localization in the presence of the background. In this paper, we also revise the optical-signal digitizer model for the ADAPT simulation based on a separate `Geant4` simulation of optical processes in a single ICC layer of ADAPT. We update the

ADAPT angular resolution for the pair-event reconstruction accordingly.

2. Modeling the Gamma-Ray and High-Energy Particle Background for ADAPT

In this study, we construct a semi-analytical gamma-ray and high-energy particle background model assuming a similar background high-energy particle intensity as measured by the Sub-MeV gamma-ray Imaging Loaded-on-balloon Experiment I (SMILE-I) [5].

The number of gamma-rays that go through a detector (N) is a function of the detector's position (x) and the gamma-ray energy (E). We have $N = N_1 + N_2$, counts where N_1 and N_2 are numbers of the diffuse cosmic and atmospheric gamma-rays, respectively. Here, we define $N_1 = \omega \cdot N_{1,\mathrm{normal}}$ and $N_2 = \eta \cdot N_{2,\mathrm{normal}}$, where $N_{1,\mathrm{normal}}$ and $N_{2,\mathrm{normal}}$ are numbers of the diffuse cosmic and atmospheric gamma-rays from zenith (i.e., $\theta = 0$), respectively. Thus, the gamma-ray spectrum, in terms of $\mathrm{d}N/\mathrm{d}E$, can be written as

$$\frac{\mathrm{d}N}{\mathrm{d}E} = \frac{\mathrm{d}N_{2,\mathrm{normal}}}{\mathrm{d}E}\left[\omega\left(\frac{1}{\beta_0} - 1\right) + \eta\right], \tag{1}$$

where $\beta_0 = \beta(\theta = 0)$. Here, we note that the spectrum of normal-incident (i.e., $\theta = 0$) atmospheric gamma-rays $\mathrm{d}N_{2,\mathrm{normal}}/\mathrm{d}E$ and the scattered component ratio β can be obtained from previous observations and models. In this work, we adopted these results from [5].

In Eq. 1, ω and η are related to incident gamma-ray vectors to the detector in the atmosphere. At a given gamma-ray energy, the differentials of the two gamma-ray components N_1 and N_2 can be written as

$$\frac{\mathrm{d}N_1}{\mathrm{d}x} = -\frac{N_1}{l} \tag{2}$$

and

$$\frac{\mathrm{d}N_2}{\mathrm{d}x} = \alpha - \frac{N_2}{l}, \tag{3}$$

where α is the secondary gamma-ray production per unit distance and l is the mean free path of gamma-rays at the position x. We assume the atmosphere consists of a finite number of layers with isotropically distributed air molecules in each layer, in which case α and l are constants within each layer. Hence, the differential equations (Eq. 2 and Eq. 3) in the i-th layer from the top of the atmosphere are given by

$$\frac{\mathrm{d}N_{1,i}}{\mathrm{d}x} = -\frac{N_{1,i}}{l_i} \tag{4}$$

$$\frac{\mathrm{d}N_{2,i}}{\mathrm{d}x} = \alpha_i - \frac{N_{2,i}}{l_i}, \tag{5}$$

where α_i and l_i are α and l in the i-th layer, respectively. For $h_0 \ll R_E$ (where h_0 is the altitude of the detector and R_E is the radius of Earth), Eq. 4 and Eq. 5 have solutions

$$N_{1,i} = N_{1,i-1}\exp\left(-\frac{x}{l_i}\right) \tag{6}$$

$$N_{2,i} = \alpha_i l_i - (\alpha_i l_i - N_{2,i-1})\exp\left(-\frac{x}{l_i}\right). \tag{7}$$

The solutions can be rewritten as

$$N_{1,i} = N_{1,0} \exp\left(-x \sum_{j=0}^{i-1} \frac{1}{l_{i-j}}\right) \tag{8}$$

$$\begin{aligned} N_{2,i} = \alpha_i l_i - \sum_{j=0}^{i-2} \left[(\alpha_{i-j} l_{i-j} - \alpha_{i-j-1} l_{i-j-1}) \exp\left(-x \sum_{k=0}^{j} \frac{1}{l_{i-k}}\right)\right] \\ -\alpha_1 l_1 \exp\left(-x \sum_{j=0}^{i-1} \frac{1}{l_{i-j}}\right) + N_{2,0} \exp\left(-x \sum_{j=0}^{i-1} \frac{1}{l_{i-j}}\right). \end{aligned} \tag{9}$$

Here, we note that $N_{1,0}$ is the total number of cosmic gamma-rays and $N_{2,0} = 0$. To simplify the calculation, we assume the atmospheric gamma-ray production rate α is proportional to the number density of air molecules. In that case, we have a constant atmospheric gamma-ray production rate per unit mean free path, assuming a fixed scattering cross section per molecule, i.e. $\alpha_i l_i = A =$ constant. Moreover, we define an effective mean free path

$$L = \left(\sum_{j=0}^{i-1} \frac{1}{l_{i-j}}\right)^{-1}. \tag{10}$$

Hence, we have

$$N_1 = N_0 \exp\left(-\frac{x}{L}\right), \tag{11}$$

and

$$N_2 \approx A \left[1 - \exp\left(-\frac{x}{L}\right)\right]. \tag{12}$$

We then obtain

$$\omega = \exp\left(\frac{h - h_0}{L} - \frac{d(\theta)}{L}\right) \tag{13}$$

for $\theta < \pi - \arcsin\left(R_E/(R_E + h_0)\right)$,

$$\omega = 0 \tag{14}$$

for $\theta \geq \pi - \arcsin\left(R_E/(R_E + h_0)\right)$, and

$$\eta \approx \frac{1 - \exp\left(-\frac{d(\theta)}{L}\right)}{1 - \exp\left(-\frac{h - h_0}{L}\right)}, \tag{15}$$

where h is the effective thickness of the atmosphere beyond which the cosmic gamma-ray attenuation and the atmospheric gamma-ray production in the atmosphere can be negligible, and $d(\theta)$ is the distance along detector's line of sight at a zenith angle θ within the effective atmosphere.

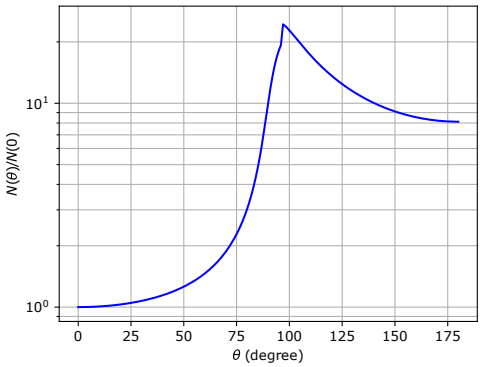

Figure 2: Zenith-angle distribution of the background gamma-rays $N(\theta)$ at energies from 100 keV to 1 GeV from our model. $N(0)$ is the gamma-ray flux at zenith angle $\theta = 0$.

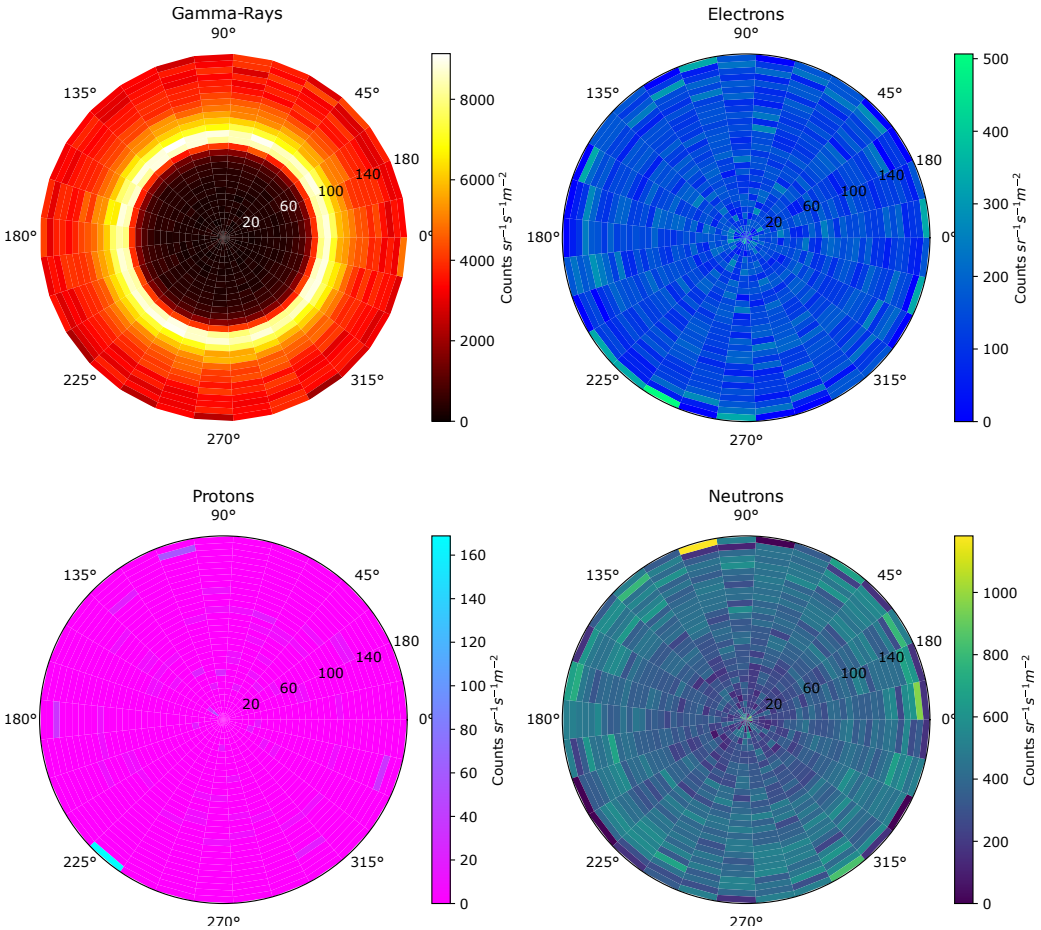

Figure 3: The ADAPT sky of gamma-rays, protons, electrons, and neutrons at energies from 100 keV to 1 GeV during a 5s exposure. The sky maps are azimuthal projected centered at the zenith. The bright ring shown in the gamma-ray sky at zenith angle $\theta \sim 0°$ shows the gamma-ray Earth's limb.

Based on the cosmic and atmospheric gamma-ray spectra and the scattered component ratio from [5], we determine the value of L and calculate the gamma-ray background rate from any direction using Eq.1, Eq.13, Eq.14, and Eq.15. We note that, for ADAPT, the zenith angle θ is the same as the inclination angle from the detector's X-Y plane. Fig. 2 shows the zenith-angle distribution of the background gamma-rays from our model. As we can see, the gamma-ray radiation peaks at $\theta \sim 90°$ from the so-called "Earth's limb". The background is dominated by the gamma-ray albedo from the atmosphere, where the flux at $\theta > 90$ is an order of magnitude larger than the zenith flux.

For high-energy particles, we consider protons, electrons, and neutrons in our background model. To simplify the calculation, we adopt the QinetiQ Atmospheric Radiation Model (QARM) [6] spectra of these components as calculated in [5], and assume a linear change over cosine zenith angle from the upward direction to the downward direction. Fig. 3 shows simulated sky maps of gamma-rays, protons, electrons, and neutrons for a 5s exposure for ADAPT. As we can see, the background for ADAPT is majorly contributed by atmospheric gamma-rays. Our current model is for an atmospheric depth of $7\,\mathrm{g}\cdot\mathrm{cm}^{-2}$.

3. Simulation of the Instrument Performance for ADAPT in the Presence of the Background

To obtain a realistic profile of optical signals captured by the WLS fibers in the ICC layers, we simulate the emission, propagation, and collection of optical photons in the CsI:Na crystals and the WLS fibers in a single layer of the ICC detector using `Geant4`. We revise the signal digitizer in our simulation of the full ADAPT detector based on the results from this optical simulation.

The APT instrument will function both as a pair telescope for 30 MeV to 1 TeV gamma-rays and as a Compton telescope with excellent sensitivity down to ~ 0.3 MeV. In the Compton regime, each reconstructed Compton event is a measure of the polar Compton angle, for which the azimuthal angle of the scatter is unknown. Thus, each reconstructed Compton event, including MeV gamma-rays from atmospheric radiation, results in a ring-shaped uncertainty region on the sky. For a gamma-ray transient such as a GRB, we localize the event by finding the centroid of the brightest region resulting from the pile-up of Compton rings in the sky map. Such a Compton map is heavily contaminated by the telluric gamma-ray and cosmic-ray radiation. To obtain the GRB-localization performance for ADAPT in the presence of the background, we simulate a large number of GRBs with spectral energy distribution described by the Band function [8] for typical short GRBs with $\alpha = -0.5$, $E_{\rm peak} = 490$ keV [9], $\beta = -2.5$, and $T_{90} = 0.3$ s. We evaluate the localization error for a range of fluence values and for multiple inclination angles from the detector's X-Y plane (i.e., the zenith angle for ADAPT).

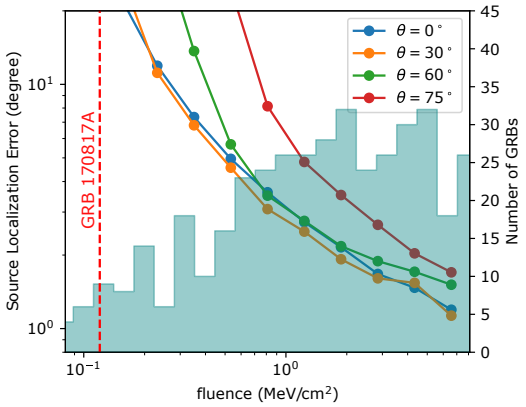

Figure 4: Error in reconstructed direction of a Band-spectrum GRB versus fluence for multiple inclination angles. The red solid and dashed line shows the estimated fluence of GRB170817A/GW170817 in the APT energy range. Histogram shows the count rate of GRBs from the first Fermi-GBM catalog [7] in the energy range from 10 keV to 1 MeV.

For each fluence value and inclination angle, we calculate the offset of the reconstructed position from the true source direction. The 68% containment of the offset angle is plotted as a function of fluence, as shown in Figure 4, where the estimated fluence of GRB170817A (an electromagnetic counterpart of the gravitational-wave event GW170817 [10]) in the APT energy range is shown as the red dashed line and the shaded region shows the count rate of GRBs from the first Fermi-GBM catalog [7] in the energy range from 10 keV to 1 MeV. As we can see, for zenith angle $\theta < 75°$, ADAPT has degree-level accuracy of localizing bright GRBs with fluence > 1 MeV/cm^{-2} in the presence of the gamma-ray and cosmic-ray background.

Based on our revised profile of optical signals captured by the WLS fibers, we update the ADAPT performance including the gamma-ray acceptance, effective area, angular resolution, and energy resolution, as shown in Fig. 5 and Fig. 6, where performances of the Fermi Space Telescope [11] and the proposed All-sky Medium Energy Gamma-ray Observatory (AMEGO) [12] are also shown for a comparison. We find that the updated ADAPT performance is generally consistent

with our prior result in [3] derived using an ideal light collection model based on the total internal reflection. We can see that even with only $\sim$ 1% of the total material of the full APT detector, ADAPT is still able to achieve an acceptable performance to observe gamma-ray sources in the MeV-GeV regime.

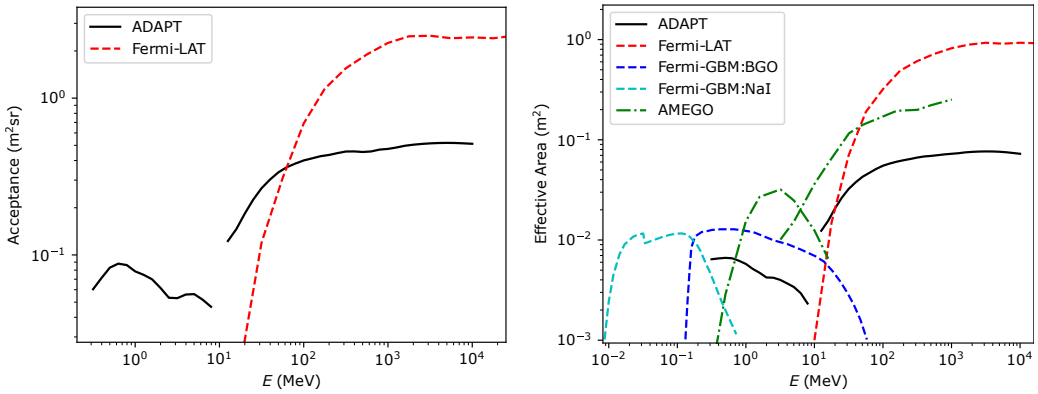

Figure 5: Acceptance/geometry factor (left) and normal-incident effective area (right) versus energy. The lower-energy solid black curves denote ADAPT Compton reconstruction and the higher denote ADAPT pair reconstruction. Dashed red and dash-dotted green curves are for *Fermi* P8R2_SOURCE_V6 events and AMEGO, respectively. Dashed blue and cyan curves show the Fermi-GBM effective area for the BGO and NaI detectors, respectively.

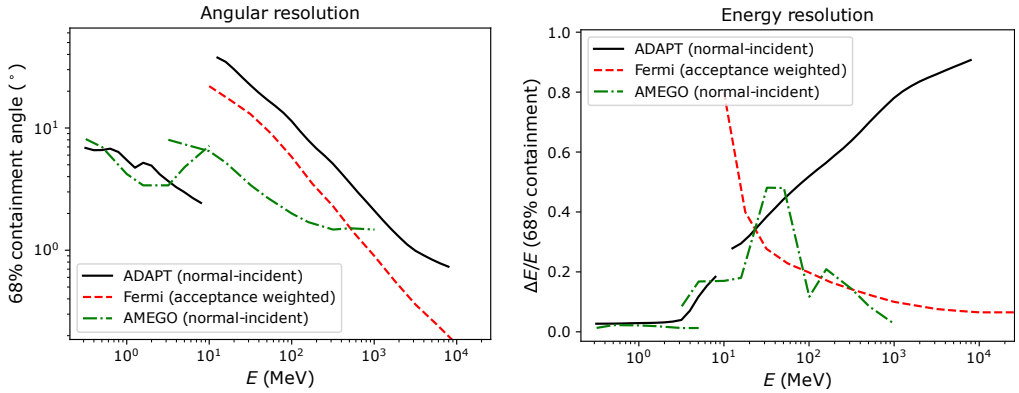

Figure 6: Angular resolution (left) and energy resolution (right) as shown by the 68% containment versus energy. Solid black curves are for ADAPT with normal-incident events. Dashed red and dash-dotted green curves are for *Fermi* P8R2_SOURCE_V6 events and AMEGO normal-incident events, respectively.

4. Summary and Discussion

In this paper, we present a model of the gamma-ray and cosmic-ray background for ADAPT. At photon energies from 30 MeV to a few GeV, ADAPT could provide degree-level to sub-degree-level observations of gamma-rays from both galactic/extragalactic gamma-ray sources and atmospheric gamma-ray radiation with an effective area of above 0.05 m^2. In the MeV regime, our simulation shows that ADAPT can achieve a degree-level localization accuracy for gamma-ray bursts down to

about 1 MeV/cm^2 in the presence of the MeV gamma-ray and cosmic-ray background. Given the distribution of the GRB fluence from Fermi-GBM observations as shown in Fig. 4, ADAPT would be able to detect a few GRBs during the planned Antarctic balloon flight.

Recently, we introduce SiPM-based *edge detectors* for ADAPT to improve the collection rate of scintillating lights from CsI:Na crystals. In this paper, however, we focus on a complete off-line analysis to derive the best reconstruction methods using WLS fiber signals in the presence of the background. To make the simulated ADAPT performance comparable to previous APT and ADAPT analyses [3], the results presented in this paper are based on the same event-reconstruction and GRB localization algorithms as used in [3]. Our preliminary modeling of the front-end electronics as well as the simulation of the light propagation in the ICC unit and light collection using the edge detectors are presented in [13]. The GRB-localization performance of ADAPT using the edge-detectors and based on the preliminary front-end computational models is described in [14].

References

[1] S. Agostinelli, J. Allison, K. Amako, J. Apostolakis, H. Araujo, P. Arce et al., *Geant4—a simulation toolkit*, *Nuclear Instruments and Methods in Physics Research Section A: Accelerators, Spectrometers, Detectors and Associated Equipment* **506** (2003) 250.

[2] J. Buckley, S.A. Nussirat, C. Altomare, J. Buhler, E. Burns, R. Chamberlain et al., *The Advanced Particle-astrophysics Telescope (APT) Project Status*, in *ICRC 2021*, Astroparticle Physics Conf., 2021.

[3] W. Chen and J. Buckley, *The Advanced Particle-astrophysics Telescope: Simulation of the Instrument Performance for Gamma-Ray Detection*, in *ICRC 2021*, Astroparticle Physics Conf., 2021.

[4] J. Buckley, *Adapt project status*, in *ICRC 2023*, Astroparticle Physics Conf., 2023.

[5] A. Takada, H. Kubo, H. Nishimura, K. Ueno, K. Hattori, S. Kabuki et al., *Observation of Diffuse Cosmic and Atmospheric Gamma Rays at Balloon Altitudes with an Electron-tracking Compton Camera*, *Astrophysical Journal* **733** (2011) 13 [1103.3436].

[6] F. Lei, A. Hands, S. Clucas, C. Dyer and P. Truscott, *Improvement to and Validations of the QinetiQ Atmospheric Radiation Model (QARM)*, *IEEE Transactions on Nuclear Science* **53** (2006) 1851.

[7] W.S. Paciesas, C.A. Meegan, A. von Kienlin, P.N. Bhat, E. Bissaldi, M.S. Briggs et al., *The Fermi GBM Gamma-Ray Burst Catalog: The First Two Years*, *The Astrophysical Journal Supplement Series* **199** (2012) 18.

[8] D. Band, J. Matteson, L. Ford, B. Schaefer, D. Palmer, B. Teegarden et al., *BATSE Observations of Gamma-Ray Burst Spectra. I. Spectral Diversity*, *Astrophys. J.* **413** (1993) 281.

[9] L. Nava, G. Ghirlanda, G. Ghisellini and A. Celotti, *Spectral properties of 438 GRBs detected by Fermi/GBM*, *Astronomy and Astrophysics* **530** (2011) A21 [1012.2863].

[10] B.P. Abbott, R. Abbott, T.D. Abbott, F. Acernese, K. Ackley, C. Adams et al., *Multi-messenger observations of a binary neutron star merger*, *The Astrophysical Journal* **848** (2017) L12.

[11] "Fermi lat performance." https://www.slac.stanford.edu/exp/glast/groups/canda/lat_Performance.htm.

[12] R. Caputo, F. Kislat, J. Racusin and O.B.O.T.A. Team, *AMEGO: Simulations of the Instrument performance*, *PoS* **ICRC2017** (2018) 783.

[13] M. Sudvarg, *Front-End Computational Modeling and Design for the Antarctic Demonstrator for the Advanced Particle-astrophysics Telescope*, in *ICRC 2023*, Astroparticle Physics Conf., 2023.

[14] Y. Htet, *Prompt and Accurate GRB Source Localization Aboard the Advanced Particle Astrophysics Telescope (APT) and its Antarctic Demonstrator (ADAPT)*, in *ICRC 2023*, Astroparticle Physics Conf., 2023.

PoS(ICRC2023)841

Full Authors List: The APT Collaboration

Corrado Altomare[12], Matthew Andrew[5], Blake Bal[7], Richard G. Bose[7], Dana Braun[7], James H. Buckley[7], Jeremy Buhler[2], Eric Burns[4], Roger D. Chamberlain[2], Wenlei Chen[6], Michael L. Cherry[4], Leonardo Di Venere[12], Jeffrey Dumonthier[13], Manel Errando[7], Stefan Funk[10], Priya Ghosh[8], Francesco Giordano[9], Jonah Hoffman[7], Ye Htet[2], Zachary Hughes[7], Aera Jung[5], Patrick L. Kelly[6], John F. Krizmanic[13], Makiko Kuwahara[3], Francesco Licciulli[12], Gang Liu[16], Leonarda Lorusso[9], Mario Nicola Mazziotta[12], John Grant Mitchell[11], John W. Mitchell[1], Georgia A. de Nolfo[11], Giuliana Panzarini[15], Richard Peschke[5], Riccardo Paoletti[17], Roberta Pillera[15], Brian Rauch[7], Davide Serini[12], Garry Simburger[7], Marion Sudvarg[2], George Suarez[13], Teresa Tatoli[11], Gary S. Varner[5], Eric A. Wulf[14], Adrian Zink[10], and Wolfgang V. Zober[7]

[1]Astroparticle Physics Laboratory, NASA/GSFC, Greenbelt, MD 20771, USA. [2]Department of Computer Science & Engineering, Washington University, St. Louis, MO 63130-4899, USA. [3]Department of Engineering, University of Hawai'i at Mānoa, Honolulu, HI 96822, USA. [4]Department of Physics and Astronomy, Louisiana State University, Baton Rouge, Louisiana 70803, USA. [5]Department of Physics and Astronomy, University of Hawai'i at Mānoa, Honolulu, HI 96822, USA. [6]Department of Physics and Astronomy, University of Minnesota, Minneapolis, MN 55455, USA. [7]Department of Physics and McDonnell Center for the Space Sciences, Washington University, St. Louis, MO 63130, USA. [8]Department of Physics, Catholic University of America, Washington DC, 20064. [9]Dipartimento di Fisica "M. Merlin" dell'Università e del Politecnico di Bari, I-70126 Bari, Italy. [10]Friedrich-Alexander-Universität Erlangen-Nürnberg, Erlangen Centre for Astroparticle Physics, D-91058 Erlangen, Germany. [11]Heliospheric Physics Laboratory, NASA/GSFC, Greenbelt, MD 20771, USA. [12]Istituto Nazionale di Fisica Nucleare, Sezione di Bari, I-70126 Bari, Italy. [13]NASA Goddard Space Flight Center, Greenbelt, MD 20771, USA. [14]Naval Research Laboratory, Washington, DC 20375, USA. [15]Politecnico di Bari, Department of Mechanics, Mathematics and Management, via Orabona, 4, I-70125 Bari, Italy. [16]SLAC National Accelerator Laboratory, 2575 Sand Hill Rd, Mailstop 0094, Menlo Park, CA 94025, USA. [17]Università di Siena and INFN Pisa, I-53100 Siena, Italy.

PoS(ICRC2023)841